# Boundary Tension Between Coexisting Phases of a Block Copolymer Blend

Russell K. W. Spencer and Mark W. Matsen*

Department of Chemical Engineering, Department of Physics & Astronomy, and the Waterloo Institute for Nanotechnology, University of Waterloo, Waterloo, Ontario, Canada

ABSTRACT: Self-consistent field theory (SCFT) is used to evaluate the excess free energy per unit area (i.e., tension) of different boundaries (or interfaces) between the coexisting phases of a block copolymer blend. In this first study of its kind, we focus on the boundaries separating the short- and long-period lamellar phases that form in mixtures of small and large symmetric diblock copolymers of polymerizations N_s and N_l, respectively, when $N_s \ll N_l$. According to strong-segregation theory (SST), the tension is minimized when both sets of lamellae orient parallel to the boundary, but experiments [Hashimoto, et al., *Macromolecules* **1994**, *27*, 1562] tend to observe kink boundaries instead, where the domains of one lamellar phase evolve continuously into those of the other lamellar phase. Our more refined SCFT calculations, on the other hand, do predict a lower tension for the kink boundary consistent with the experimental observations. For completeness, we also examine the boundaries that form when the short-period lamellar phase disorders, and again the SCFT results are in agreement with experiment.

$N_s/N_l \approx 0.06$
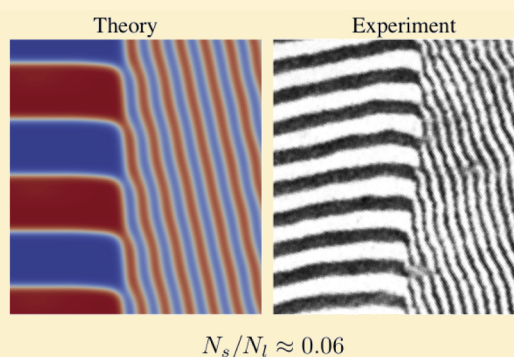
INTRODUCTION

Block copolymers are being used in an expanding range of applications,[1] often in the form of blends[2,3] for the simple reason that their morphology (or microstructure) is more easily controlled by adjusting a blend ratio than changing molecular parameters,[4,5] which requires synthesizing new molecules. While neat block copolymer materials typically form polycrystalline morphologies consisting of regions (or grains) with different orientations of the same ordered phase,[6] blends can also involve regions (or macrodomains) of different ordered phases. In both cases, the size and shape of the coherent regions are affected not only by how the material is prepared (e.g., annealing time, annealing temperature, use of solvent, etc.), but also by the tension along their boundaries.[7] As for simple uniform phases, a higher boundary tension leads to larger regions. However, when the phases possess microstructure, then the tension depends upon the relative orientations between the boundary and the phases, and this affects the shape of the regions.

There have been several theoretical studies on the grain boundaries in neat diblock copolymer melts.[8−10] Even though they have focused on the simple lamellar phase, the behavior has proven to be extraordinarily rich. However, there have yet to be any analogous studies for blends, where the boundaries separate different coexisting phases. Admittedly, there are some studies of the boundaries between different ordered phases of a neat diblock copolymer melt,[11−13] but this is a dynamical problem as one phase is always more stable than the other causing the boundary to propagate. On the other hand, a blend can exhibit coexisting phases resulting in stable boundaries, like the grain boundaries of a neat melt. The added complication, though, is that a blend involves a number of distinct molecular species, which is the challenge we will address in this paper.

In the interest of starting off with the simplest system possible, we consider a blend of small and large symmetric AB diblock copolymers. This system has, in fact, proven to be particularly intriguing. Calculations[14] using strong-stretching theory (SST)[15] initially predicted that such blends would never macrophase separate under any condition. Shortly after, however, experiments by Hashimoto et al.[16,17] observed coexisting short- and long-period lamellar (LAM) phases, when the size ratio of the two diblocks exceeded 1:10. This contradiction was soon resolved with more accurate calculations,[18] using self-consistent field theory (SCFT),[19] where the predicted phase diagrams (see Figure 1) exhibited the macrophase separation seen in the experiments. This success was then eclipsed by subsequent experiments,[20] which demonstrated stunning quantitative agreement with the SCFT predictions.

In addition to the macrophase separation, Hashimoto et al.[17] also documented a number of distinct boundaries between the coexisting LAM phases. The most common was a kink boundary, where the A- and B-rich domains of the two LAM phases remain connected through the boundary. In its most general form depicted in Figure 2a, the short- and long-period LAM phases are oriented at angles $\theta^{(s)}$ and $\theta^{(l)}$ to the boundary, respectively. For the domains to match up, the angles must satisfy
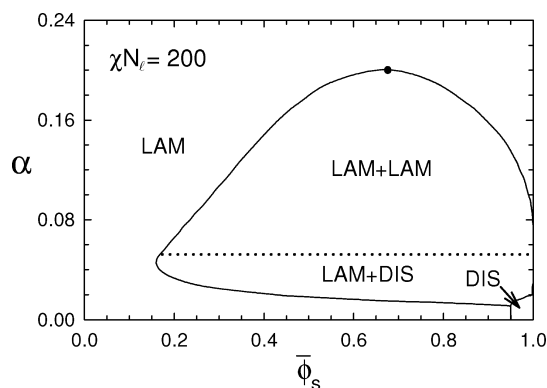
Figure 1. Phase diagram for blends of small and large symmetric AB diblock copolymers[18] plotted in terms of their size ratio, $\alpha = N_s/N_l$, and the volume fraction of small diblocks, $\bar{\phi}_s$. The segregation strength of the large diblocks is fixed at $\chi N_l = 200$. The dot denotes a critical point, below which the blend separates into coexisting short- and long-period lamellar (LAM) phases, and the dotted line is an order−disorder transition (ODT), below which the short-period LAM phase switches to a disordered (DIS) phase.
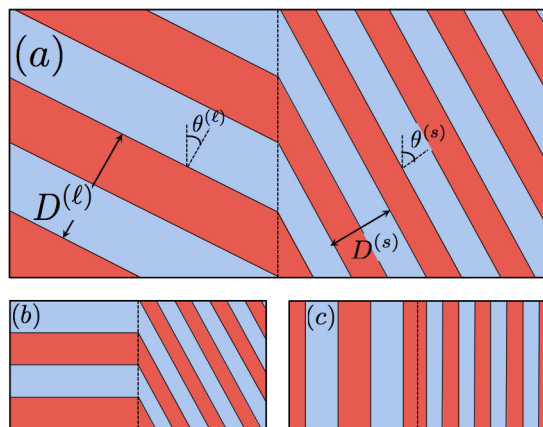
Figure 2. (a) Kink boundary between the short- and long-period LAM phases. The continuity of the A- and B-rich domains requires the lamellar orientations, $\theta^{(s)}$ and $\theta^{(l)}$, and periods, $D^{(s)}$ and $D^{(l)}$, to satisfy eq 1. (b) One-sided inclination version of the kink boundary observed in experiment.[17] (c) Parallel boundary favored by SST.

$$\frac{D^{(s)}}{\cos(\theta^{(s)})} = \frac{D^{(l)}}{\cos(\theta^{(l)})} \tag{1}$$

where $D^{(s)}$ and $D^{(l)}$ are the bulk periods of the respective phases. Although this avoids creating any excess A/B interface, the boundary cuts diagonally through the lamellae. In SST, where the diblock copolymers extend normal to the A/B interface, this forces the polymers to rearrange the way they fill space. To minimize the resulting free energy cost, the system will reduce the kink angle as much as possible. The best it can do is orient the large lamellae perpendicular to the boundary (i.e., $\theta^{(l)} = 0$) as depicted in Figure 2b, which in turn minimizes $\theta^{(s)}$. Indeed, this *one-sided inclination* version of the kink boundary is exactly what experiments typically observe.[17] Although this all seems very reasonable, simple SST-based reasoning would suggest that the most favorable boundary is the parallel version depicted in Figure 2c, where both sets of lamellae are oriented parallel to the boundary (i.e., $\theta^{(s)} = \theta^{(l)} = 90°$). According to SST, the tension of such a boundary would be exactly zero, and thus it is rather perplexing that it has not

even been observed. Another puzzling result occurs when the short-period LAM phase disorders. Assuming the remaining LAM phase is well ordered, SST suggests that its lamellae would select one of two equally preferred orientations, either parallel or perpendicular to the boundary.[21] While experiments[16,17] observe the perpendicular version of the LAM + DIS boundary, there has been no sign of the parallel orientation.

The failure of SST to account for the experimental observations may be because the selection of boundaries has more to do with the kinetics of macrophase separation than the boundary tension. Alternatively, it could just be that SST does not provide a sufficiently accurate treatment of the boundaries, as was the case for the macrophase separation itself. To shed some light on this, we now compare the different boundaries using the more refined SCFT.

■ THEORY

This section describes the self-consistent field theory (SCFT) for the coexisting phases of a binary blend consisting of n_s small AB diblock copolymers of polymerization N_s and n_l large AB diblock copolymers of polymerization N_l. Here the polymerization of the large diblock, N_l, is chosen as our reference, and the relative size of the small diblock is specified by $\alpha \equiv N_s/N_l$. In this particular study, all diblocks have a symmetric composition with an equal number of A- and B-type segments. As usual, we assume an incompressible melt, where each segment occupies a volume of ρ_0^{-1} and where the A and B segments are conformationally symmetric with a common segment length of a. The incompressibility implies that the volume of our system is fixed at $V = (n_s N_s + n_l N_l)/\rho_0$. The interaction between the unlike segments is controlled by the standard Flory−Huggins χ parameter.

The difference between the boundaries in a blend and the grain boundaries in a neat melt is that each molecular species of the blend will exhibit either an excess or depletion at a boundary. Although these excesses (or depletions) will adjust automatically in the grand-canonical ensemble,[22] this ensemble also allows the position of the boundary to move freely, which compromises the numerical stability of the calculation. Consequently, we are forced to use the canonical ensemble, where the position of the boundary is constrained by the blend composition.

In the canonical ensemble, the A- and B-segment concentrations, $\phi_{\gamma,A}(\mathbf{r})$ and $\phi_{\gamma,B}(\mathbf{r})$, and the single-chain partition function, Q_γ, are calculated for short and long diblocks (i.e., $\gamma = s$ and l, respectively) using the same expressions as for neat diblocks.[23] We solve the necessary diffusion equations for this part of the calculation using the pseudospectral algorithm developed by Ranjan et al.[24] Of course, to properly fill the volume V, the concentrations of the small and large diblocks must be scaled by factors of $\bar{\phi}_s$ and $(1 - \bar{\phi}_s)$, respectively, where $\bar{\phi}_s \equiv n_s N_s/\rho_0 V$ is the composition of the blend. The next step is to adjust the fields acting on the A and B segments to satisfy the self-consistent conditions,

$$w_A(\mathbf{r}) = \chi N_l \phi_B(\mathbf{r}) + \xi(\mathbf{r}) \tag{2}$$

$$w_B(\mathbf{r}) = \chi N_l \phi_A(\mathbf{r}) + \xi(\mathbf{r}) \tag{3}$$

where $\phi_\delta(\mathbf{r}) \equiv \phi_{s,\delta}(\mathbf{r}) + \phi_{l,\delta}(\mathbf{r})$ for δ = A or B and $\xi(\mathbf{r})$ is the pressure field used to enforce the incompressibility condition, $\phi_A(\mathbf{r}) + \phi_B(\mathbf{r}) = 1$. This is done using an Anderson mixing scheme devised earlier.[25] Once the field equations are satisfied, the free energy of the system is evaluated using

$$\frac{FN_l}{k_B T \rho_0 V} = (1 - \bar{\phi}_s) \ln\left(\frac{1 - \bar{\phi}_s}{Q_l}\right) + \frac{\bar{\phi}_s}{\alpha} \ln\left(\frac{\bar{\phi}_s}{Q_s}\right)$$
$$+ \frac{1}{V} \int [\chi N_l \phi_A(\mathbf{r}) \phi_B(\mathbf{r}) - w_A(\mathbf{r}) \phi_A(\mathbf{r}) - w_B(\mathbf{r}) \phi_B(\mathbf{r})] \, d\mathbf{r}$$

$$(4)$$

Before considering the phase boundary, it is necessary to first calculate the free energy, F, and period, D, of the bulk LAM phase as a function of the blend composition, $\bar{\phi}_s$, at fixed α. Figure 3 shows a sample calculation for $\alpha = 0.06$. From the
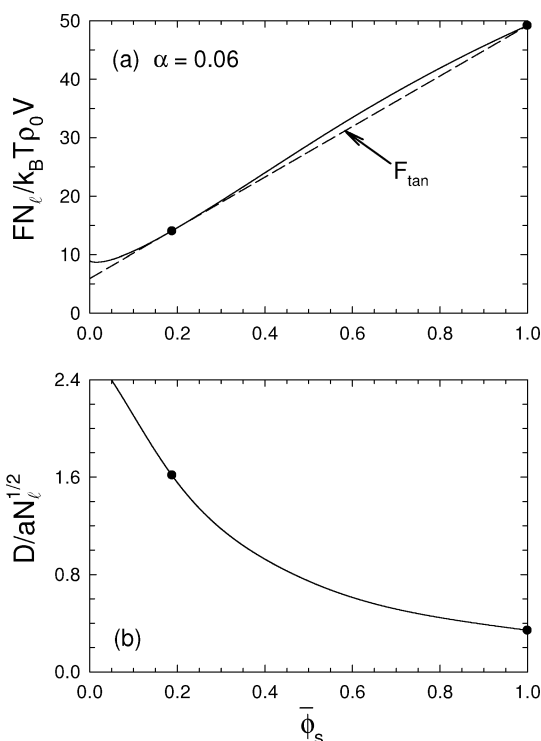
Figure 3. (a) Free energy, F, and (b) period, D, of a LAM phase plotted versus the blend composition, $\bar{\phi}_s$, for $\chi N_l = 200$ and $\alpha = 0.06$. The dots denote the binodal points determined by the double-tangent line, F_{tan}, in the upper plot.

double tangent, F_{tan}, denoted by the dashed line in Figure 3a, we obtain the compositions, $\bar{\phi}_s^{(\gamma)}$, and periods, $D^{(\gamma)}$, of the coexisting phases ($\gamma = s$ and l) indicated by dots in Figure 3. With that information in hand, we then choose a system box with appropriate boundary conditions (BC's) for the diffusion equations and construct initial guesses for the fields, $w_\delta(\mathbf{r})$.

Figure 4a shows a suitable system box for the parallel LAM + LAM boundary. Given that there is no variation in the lateral direction, the diffusion equations just have to be solved in one dimension (i.e., $0 \leq x \leq L$). This is done with reflecting BC's, which constrains the center of a lamellar domain to each end of the box, $x = 0$ and L. Of course, the box has to be large enough that the lamellae at the ends acquire bulk characteristics; we always repeat our calculations for a range of L values so as to ensure that our results are free of any noticeable finite-size effects. To construct initial guesses for $w_\delta(\mathbf{r})$, we simply splice the bulk solutions together with a boundary at an $x=x_b$ near the middle of the box. The blend composition is set to $\bar{\phi}_s = [x_b \, \bar{\phi}_s^{(l)} + (L-x_b)\bar{\phi}_s^{(s)}]/L$. The field eqs 2 and 3 are then solved, and the boundary tension, Γ_b, is obtained from the free energy excess per unit area,
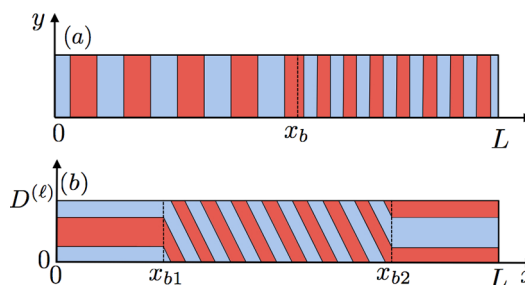
Figure 4. System boxes for the (a) parallel and (b) kink boundaries. The former boundary (at $x = x_b$) just involves a 1D calculation using reflecting BC's (at $x = 0$ and L). However, the later case requires a 2D calculation with two boundaries (at $x = x_{b1}$ and x_{b2}) using reflecting BC's in the x-direction (at $x = 0$ and L) and periodic BC's in the y-direction (at $y = 0$ and $D^{(l)}$).

$$\frac{\Gamma_b N_l^{1/2}}{k_B T \rho_0 a} = \min_{L, \bar{\phi}_s} \left(\frac{(F - F_{tan}) N_l}{k_B T \rho_0 V} \times \frac{L}{a N_l^{1/2}} \right)$$

$$(5)$$

To equilibrate the system requires minimization with respect to L, which allows the lamellae to relax to their preferred thicknesses, and with respect to $\bar{\phi}_s$, which optimizes the excess (or depletion) of small diblock at the boundary.

Figure 4b displays an appropriate system box for the kink boundary. In this case, the box contains two boundaries at $x = x_{b1}$ and x_{b2} with the short-period LAM phase between and long-period LAM phases to either side. As before, initial guesses for $w_\delta(\mathbf{r})$ are constructed from the bulk solutions and the composition is set to $\bar{\phi}_s = [(L + x_{b1} - x_{b2})\bar{\phi}_s^{(l)} + (x_{b2} - x_{b1})\bar{\phi}_s^{(s)}]/L$. Periodic BC's are applied in the y-direction, which forces the boundaries to orient perpendicular to the x-direction. Setting the box size in the y-direction to $D^{(l)}$ forces the long-period LAM phase to orient with $\theta^{(l)} = 0$, which allows us to apply reflecting BC's in the x-direction. For this particular set up, the boundary tension is given by

$$\frac{\Gamma_b N_l^{1/2}}{k_B T \rho_0 a} = \frac{1}{2} \times \frac{(F - F_{tan}) N_l}{k_B T \rho_0 V} \times \frac{L}{a N_l^{1/2}}$$

$$(6)$$

where the factor of one-half accounts for the fact that the system box contains two boundaries. Because the long-period lamellae can vary their length to fit the box, there is no need to minimize Γ_b with respect to L. Although the system still needs to adjust the excess (or depletion) of short diblock at the two boundaries, this does not actually require a minimization with respect to $\bar{\phi}_s$. The system does this automatically by changing the relative volumes of the two coexisting phases, which is made possible by the fact that the two long-period LAM regions can shift in the y-direction independently of each other.

We follow analogous procedures when the short-period LAM phase disorders producing LAM+DIS coexistence, but there are a couple of simplifications. For the parallel boundary, the minimization in eq 5 only needs to be done with respect to either L or $\bar{\phi}_s$, but not both. For the perpendicular case, we reduce the size of the system box so that it just contains one boundary, in which case the factor of a half is dropped from eq 6.

■ RESULTS

The SCFT is now applied to boundaries corresponding to the coexistence regions in Figure 1, where the level of segregation for the large diblock copolymer is fixed at $\chi N_l = 200$ while the

level of segregation for the small diblock copolymer varies as $\chi N_s = 200\alpha$. The study is broken into three parts. It begins by examining the morphology of the order—order boundaries, then that of the order—disorder boundaries, and concludes by comparing their excess free energies per unit area (i.e., tensions).

LAM + LAM Boundaries. We start by examining the parallel boundary depicted in Figure 2c, where the concentration profiles only depend on x. Figure 5 plots both the total
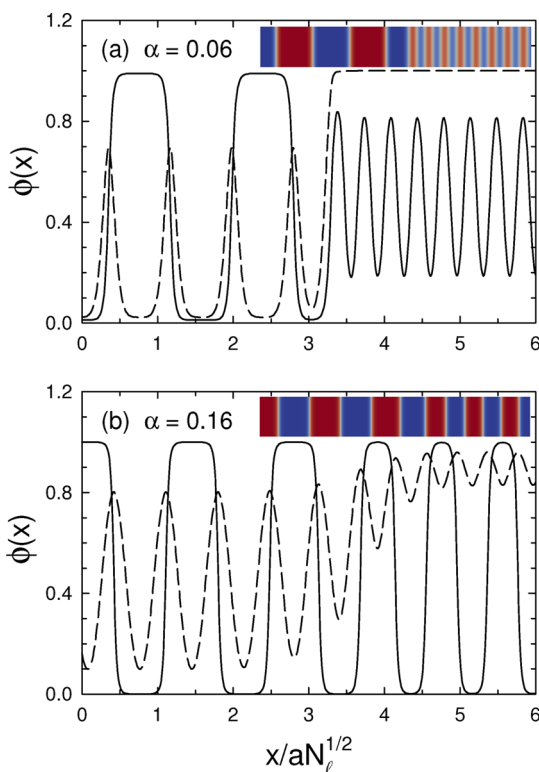
Figure 5. Total A concentration, $\phi_A(x)$, (solid curves) and total small-diblock concentration, $\phi_s(x)$, (dashed curves) plotted across the parallel LAM + LAM boundary for blends with (a) $\alpha = 0.06$ and (b) $\alpha = 0.16$. The insets show 2D color plots of $\phi_A(\mathbf{r})$, analogous to the ones that we will use to illustrate kink boundaries.

concentration of A segments (solid curves) and the concentration of the small diblocks (dashed curves) for a blend with $\alpha = 0.06$, where the two LAM phases have very distinct periods, and for $\alpha = 0.16$, where the coexisting LAM phases are relatively similar. For the smaller α, the coexistence is between an essentially pure small-diblock LAM phase at a weak segregation of $\chi N_s = 12$ and a strongly segregated LAM phase consisting mostly of large diblocks but also a significant amount of small diblock concentrated at the A/B interfaces. The compositions, $\bar{\phi}_s^{(s)}$ and $\bar{\phi}_s^{(l)}$, of the two phases are, of course, consistent with the binodal curves of the LAM+LAM region in Figure 1. In Figure 5b, where α is just below the critical point, both LAM phases are well segregated and contain substantial amounts of both diblock species.

As evident from the profiles in Figure 5a, the boundary is relatively sharp for $\alpha = 0.06$. In fact, the long-period LAM phase is virtually indistinguishable from the bulk phase within one period of the boundary. The short-period LAM phase takes a couple periods to reach its bulk properties, partly because each period corresponds to a shorter distance and also because it is

less segregated. However, the width of the boundary diverges as the critical point is approached (i.e., $\alpha \rightarrow \alpha_c^-$). To gauge the width of the boundary in Figure 5b for $\alpha = 0.16$, Figure 6 plots
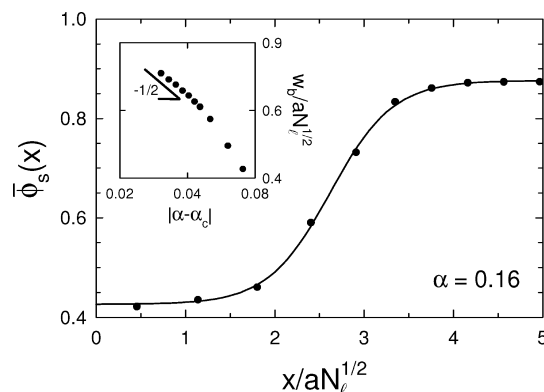
Figure 6. Average composition of the microdomain layers (dots) plotted across the parallel LAM + LAM boundary for a blend with $\alpha = 0.16$. The curve is a fit to eq 7, from which we extract the width of the boundary, w_b. The inset shows a log—log plot demonstrating that w_b diverges at the critical point following a power-law, eq 8, with an exponent of $\nu = \frac{1}{2}$.

the average composition, $\bar{\phi}_s$, of each microdomain layer as a function of its position. (Note that the edges of the microdomains are defined by $\phi_A(x) = 0.5$ and the microdomain positions are defined by their centers.) The width of the boundary, w_b, is then extracted by fitting the points to a hyperbolic tangent function

$$\bar{\phi}_s(x) = \frac{1}{2}(\bar{\phi}_s^{(s)} - \bar{\phi}_s^{(l)}) \tanh\left(\frac{2(x - x_b)}{w_b}\right)$$
$$+ \frac{1}{2}(\bar{\phi}_s^{(s)} + \bar{\phi}_s^{(l)}) \tag{7}$$

This symmetric fitting function assumes that $\bar{\phi}_s(x)$ converges to the bulk values, $\bar{\phi}_s^{(l)}$ and $\bar{\phi}_s^{(s)}$, at the same rate on both sides of the boundary, but this is a good approximation near the critical point. The inset in Figure 6 shows a log—log plot of the width, w_b, versus distance from the critical point, $|\alpha - \alpha_c|$, and the straight-line segment illustrates that the width diverges as a power-law,

$$w_b \propto |\alpha - \alpha_c|^{-\nu} \tag{8}$$

with a critical exponent of $\nu = \frac{1}{2}$. This is the usual mean-field exponent for boundaries between two coexisting phases, including the simple boundary between two immiscible homopolymers.[26]

Now we move onto the kink boundary depicted in Figure 2b. In this case, the morphology varies in both the x- and y-direction, and so Figure 7 plots the total A-segment concentration, $\phi_A(\mathbf{r})$, in 2D using a color scale. The distribution of small diblocks is essentially equivalent to that of the parallel boundary, and so we do not include an extra plot for $\phi_s(\mathbf{r})$. At $\alpha = 0.06$, where there is a significant size difference between the lamellar periods, the thick lamellae possess relatively square ends, each with a thin lamella emerging from one of their corners. The lamellae of the short-period phase then develop ripples in order to keep their domains relatively uniform in thickness, while accommodating the square ends of the large lamellae. These ripples fade toward the bulk, but nevertheless
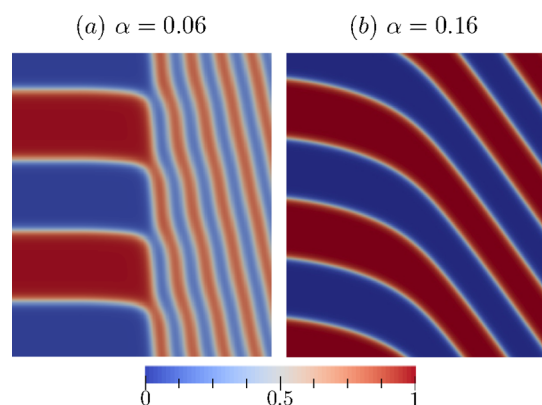
Figure 7. Total A-segment concentration, $\phi_A(\mathbf{r})$, plotted across the kink LAM + LAM boundary for blends with (a) $\alpha = 0.06$ and (b) $\alpha = 0.16$. Each image is 3.0×3.5 in units of $aN_l^{1/2}$, and the color scale is shown at the bottom.

they do persist for a considerable distance from the boundary. We note that these ripples are clearly evident in the experimental TEM images,[17] including the one displayed in the Abstract graphic.

As the critical point is approached and the two LAM phases become similar, the kink angle decreases and the width of the boundary diverges again. As before, we gauge the width by examining the change in the average blend composition, $\bar{\phi}_s(x)$, plotted in Figure 8 for $\alpha = 0.16$. In this case, we just average
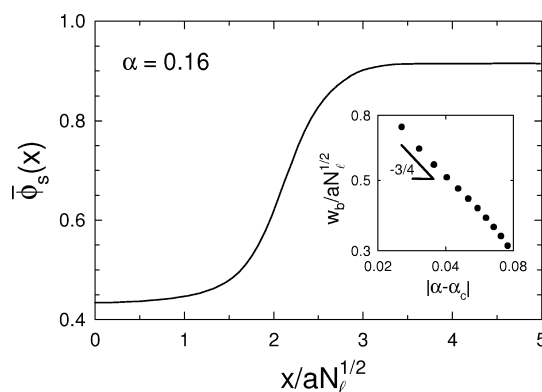
Figure 8. Analogous plot to Figure 6, but for the kink LAM + LAM boundary at $\alpha = 0.16$. In this case, the composition, $\bar{\phi}_s(x)$, is obtained by averaging the concentration of small diblock, $\phi_s(\mathbf{r})$, parallel to the boundary. Again the inset shows a power-law divergence in the width of the boundary, eq 8, but with an exponent of $\nu = {}^3/_4$.

$\phi_s(\mathbf{r})$ in the lateral y-direction, which gives a continuous curve in the x-direction. Near the critical point, $\bar{\phi}_s(x)$ is virtually indistinguishable from the hyperbolic tangent function in eq 7, which we use to extract the width, w_b. The log−log plot in the inset of Figure 8 illustrates a power-law divergence, eq 8, but this time it occurs with a critical exponent of $\nu = {}^3/_4$ that is distinctly larger than the usual value of $\nu = {}^1/_2$. The new exponent, however, is readily accounted for by a simple analytical calculation described in the Appendix.

LAM + DIS Boundaries. It is interesting to extend our calculations to the analogous boundaries at smaller α, where the short-period LAM phase disorders. Figure 9 plots the concentration of A segments (solid curves) and small diblock (dashed curve) across the parallel LAM + DIS boundary for
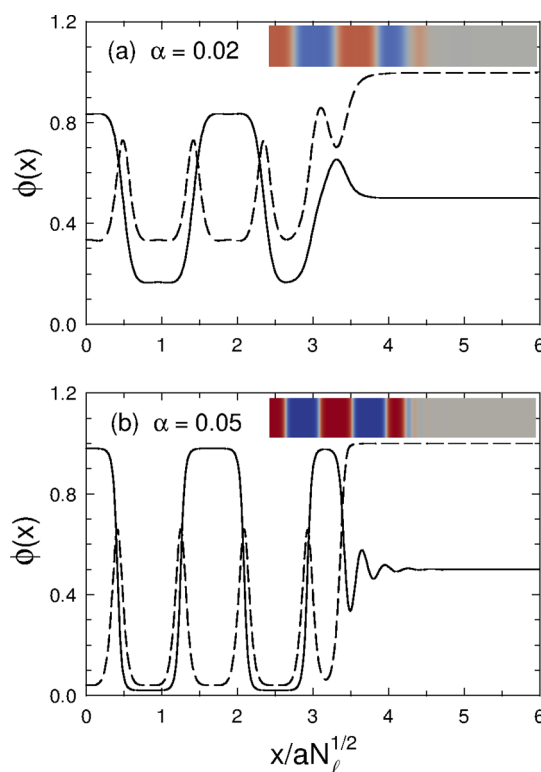

Figure 9. Analogous plots to Figure 5, but for the parallel LAM+DIS boundary at (a) $\alpha = 0.02$ and (b) $\alpha = 0.05$.

blends with $\alpha = 0.02$ and 0.05. Consistent with the binodal curves in Figure 1, the DIS phase is nearly pure small diblock. While the LAM phase is rich in large diblocks, it does contain a substantial amount of small diblock. The amount also increases as α decreases, because smaller molecules gain more translational entropy per unit volume by penetrating into the LAM phase. Although the small diblocks still accumulate at the A/B interface, for the most part they uniformly dilute the large diblocks, which then tends to disorder the LAM phase.[27] Figure 10 shows the perpendicular LAM + DIS boundary, where the lamellae are oriented perpendicular to the boundary. We see that the truncated lamellae have reasonably square ends at larger α, but that the ends become somewhat rounded at smaller α.
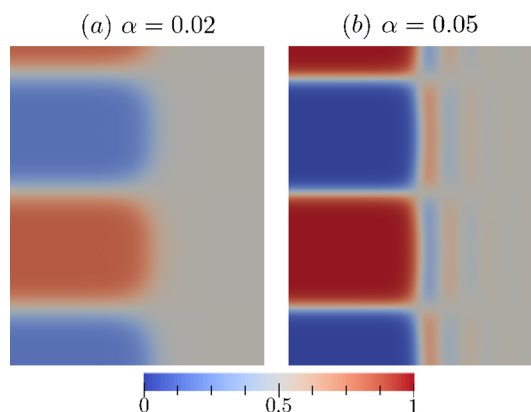
Figure 10. Analogous plots to Figure 7, but for the perpendicular LAM+DIS boundary at (a) $\alpha = 0.02$ and (b) $\alpha = 0.05$.

As evident in Figures 9b and 10b, the ordered LAM phase induces short-range order in the DIS phase. This is illustrated more clearly in Figure 11, where the A-segment concentration,
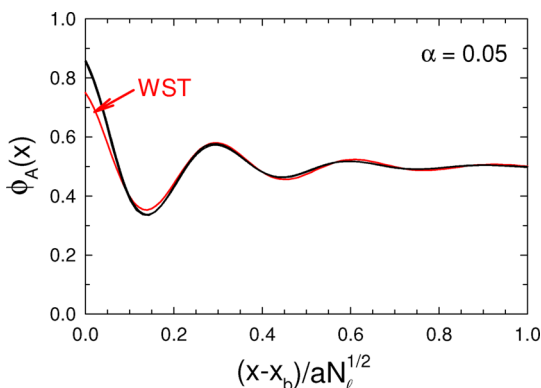
Figure 11. Total A-segment concentration, $\phi_A(\mathbf{r})$, plotted from the boundary into the DIS phase for $\alpha = 0.05$. SCFT results for the parallel and perpendicular boundaries, Figures 9b and 10b, respectively, are plotted with black curves (indistinguishable on this scale), and the WST approximation from eq 9 is shown with a red curve.

$\phi_A(x)$, in the DIS phase is plotted as a function of distance, $x - x_b$, from the boundaries. (For the perpendicular boundary, the profile is plotted along a line extending through the center of an A-rich lamella.) The profiles from both boundaries are so similar that they appear indistinguishable on the scale of our plot, so long as we adjust x_b appropriately.

The profiles in Figure 11 are reminiscent of the surface ordering examined by Fredrickson[28] for disordered diblock copolymer melts next to a preferential surface. Using an approximation to weak-segregation theory (WST),[29] Fredrickson predicted exponentially decaying oscillations,

$$\phi_A(x) = A_0 \exp(-x/\zeta) \cos(kx + \phi_0) \tag{9}$$

where in the case of symmetric molecules (i.e., $f = 0.5$) the decay length is given by

$$\frac{\zeta}{aN^{1/2}} = \left[\frac{3}{2}(10.495 - \chi N) \right]^{-1/2} \tag{10}$$

and the wavevector of the oscillation is

$$kaN^{1/2} = \left[\frac{3}{2}(\chi N - 10.495 + 8\sqrt{3}) \right]^{1/2} \tag{11}$$

Because our disordered phase is nearly pure, we can apply this prediction with N replaced by N_s. Given that $\chi N_s = 10$ for $\alpha = 0.05$, it follows that $\zeta/aN_s^{1/2} = 1.16$ and $kaN_s^{1/2} = 4.48$. The red curve in Figure 11 is fit to eq 9 using these values of ζ and k while adjusting A_0 and ϕ_0. Considering the approximations involved, this prediction by Fredrickson captures the effect rather well.

Boundary Tensions. Now that we have finished examining the morphologies of our candidate boundaries, Figure 12 compares their tensions as a function of α. The comparison reveals that the kink boundary is preferred over the parallel boundary in the LAM + LAM region ($\alpha_{ODT} < \alpha < \alpha_c$), apart from a small interval near the critical point where their tensions are similarly small. Likewise, the perpendicular boundary has a lower tension than the parallel boundary in the LAM+DIS
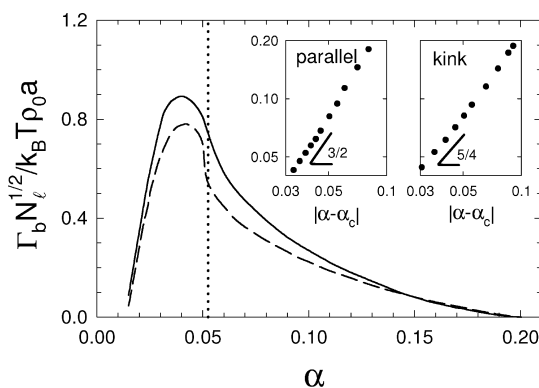
Figure 12. Tensions of the parallel (dashed curve) and perpendicular/kink (dashed curve) boundaries versus relative size of the diblocks. The vertical dotted line denotes the ODT from Figure 1, and the insets demonstrate a power-law dependence near the critical point, eq 12, with exponents $\mu = {}^3/_2$ and ${}^5/_4$, respectively.

region ($\alpha < \alpha_{ODT}$). Both results are consistent with what is most commonly observed in experiment.

The tensions of the parallel LAM + LAM and LAM + DIS boundaries (Figures 5 and 9, respectively) form a continuous curve across the ODT (dotted line in Figure 12). This is because the short-period LAM phase evolves continuously into the DIS phase on account of the ODT being a second-order transition. However, it is less obvious that the tensions of the kink LAM + LAM and perpendicular LAM + DIS boundaries are continuous across the ODT, because it is not immediately clear how the morphology of the kink boundary with its connected short-period lamellae (see Figure 7a) would evolve smoothly into the perpendicular boundary with its disconnected domains in the DIS phase (see Figure 10b). From calculations very close to the ODT, it appears that the thin lamellae begin pinching off starting next to the boundary and then extending outward as $\alpha \rightarrow \alpha_{ODT}^+$. In this way, the kink boundary does transform continuously into the perpendicular boundary across the ODT.

In the other direction, $\alpha \rightarrow \alpha_c^-$, the tension of both LAM + LAM boundaries must vanish, since the coexisting LAM phases become identical at the critical point. As usual for critical points, the tension should vanish following a power-law,

$$\Gamma_b \propto |\alpha - \alpha_c|^\mu \tag{12}$$

with some critical exponent, μ. The insets in Figure 12 illustrate that the parallel boundary is consistent with the usual critical exponent of $\mu = {}^3/_2$,[26] while the kink boundary is consistent with the smaller exponent of $\mu = {}^5/_4$ derived in the Appendix. Although the difference in μ is not as pronounced as that of ν for the boundary width in eq 8, the difference is undoubtedly real because each pair of exponents should satisfy the relation $\mu + \nu = 2$.[30]

■ DISCUSSION

This study is the first to demonstrate the application of SCFT to boundaries between coexisting ordered phases in a block copolymer blend. In principle, blends are most easily treated in the grand-canonical ensemble, where the composition adjusts automatically, avoiding the need to minimize the excess free energy with respect to the composition, $\bar{\phi}_s$. In this ensemble, however, it proves difficult to converge the self-consistent field eqs 2 and 3. We attribute the difficulty to the fact that the

relative amounts of the coexisting phases are free to vary, which allows the boundary to drift. Furthermore, any inaccuracy in the chemical potential exacerbates the problem, in that it gives one phase a slight preference over the other, causing it to consume the entire system box. In the canonical ensemble, on the other hand, the relative amounts of the two phases are constrained by the fix composition, $\bar{\phi}_s$. In some cases, it is not even necessary to minimize Γ_b with respect to $\bar{\phi}_s$, but even if it is, the extra computational cost is minimal and certainly worth the added numerical stability. In reality, the most important consideration in regards to numerical cost is finding the smallest possible system box with appropriate boundary conditions (BC's) in which to solve the diffusion equations of SCFT.

SCFT continues to build up an impressive track-record in regards to blends of small and large symmetric diblock copolymers, particularly in comparison to SST. First, the SCFT prediction for the distribution of small and large diblocks within a LAM phase is in good agreement with experiment,[31] far more so than that of SST.[32,33] Second, SCFT predicts the LAM+LAM and LAM+DIS coexistence[18] with amazing accuracy,[20] whereas SST fails to even anticipate the macrophase separation.[14] Now we see that SCFT favors the kink boundary observed in experiments[17] over the parallel boundary favored by SST.

Although SST is not expected to be quantitatively accurate, it has a reputation for providing reliable qualitative explanations for phase behavior.[34] In the strong-segregation limit, the free energy of the individual monolayers of the lamellar phase are independent of each other, and thus there is no energetic penalty for placing a thin monolayer next to a thicker monolayer, which is why SST predicts zero tension for the parallel boundary. On the other hand, there is an energetic cost to truncating a monolayer at an angle to the lamellar normal (i.e., $\theta^{(\gamma)} \neq 0$). In the SST, the polymer chains extend perpendicular to the A/B interface, and thus a nonzero $\theta^{(\gamma)}$ requires the rearrangement of chain trajectories, which in turn causes packing frustration.[23] Although this is avoided in the long-period phase by having $\theta^{(l)} = 0$, the short-period phase still requires $\theta^{(s)} > 0$ in order to maintain the continuity of the domains. Thus, the packing frustration cannot be completely eliminated, and so SST will necessarily predict a positive tension for the kink boundary. Although the relative stability of the parallel and kink boundaries is opposite to what our SCFT calculation predicts, it is known that SCFT converges to SST in limit of $\chi \rightarrow \infty$,[35] and so our SCFT prediction must eventually reverse at sufficiently high segregation.

There is no simple explanation of why SCFT predicts a lower tension for the kink boundary than the parallel boundary. After all, qualitative explanations for block copolymer phase behavior are generally based upon the SST description. The fact that SCFT predicts the opposite to SST implies that the explanation is a subtle one related to the finite segregation of the melt. It may seem plausible that an explanation could be found by decomposing the excess free energy of the boundaries into various contributions, such as enthalpy, stretching energies of the blocks, and translational entropy of the junction points.[34] While such excesses are well-defined for a grain boundary between the same phase, they are not for boundaries between different phases. In the later case, where the free energy contributions have different values in the neighboring phases, the excesses depend on how one defines the position of the boundary, x_b. Unfortunately, there is no definitive definition of x_b, particularly when the width of the boundary, w_b, is

comparable to the lamellar periods. The only excess that is unambiguous is that of the total grand-canonical free energy (i.e., the boundary tension).

We have assumed, based on experimental evidence and some rational arguments, that the long-period LAM phase is perpendicular to the boundary (i.e., $\theta^{(l)} = 0$). The tension, however, might decrease somewhat when the large lamellae are slightly tilted relative to the boundary. In principle, the SCFT could be solved with both LAM phases tilted provided we implemented periodic BC's in both the x- and y-directions. However, the long-period phase would have to wrap around the periodic BC's in the y-direction at least once, which for small tilt angles would require a very large system size in the x-direction. Unfortunately this is not computationally feasible. Alternatively, it may seem conceivable that the semianalytical calculation in the Appendix could address this issue. However, that calculation is only valid near the critical point where the two phases are nearly identical. In this limit, the tension becomes insensitive to the orientation of the boundary, and unfortunately this results in very small energy variations which the analytical treatment is not sufficiently accurate to resolve.

While the experiments[16] reported evidence of macrophase separation when the size ratio exceeded 1:5 (i.e., $\alpha \lesssim 0.2$), they only observed LAM + LAM coexistent for size disparities beyond about 1:10 (i.e., $\alpha \lesssim 0.1$). This is readily explained by our prediction that the boundary tension vanishes and the boundary width diverges as the critical point is approached. The lower tensions will result in smaller bulk regions and the increased width will make the regions less discernible. Thus, if the experiments are not sufficiently far from the critical point, they will likely just observe what appears to be a poorly ordered LAM phase consisting of wavy lamellae with a fluctuating domain thickness.

While the kink boundary has a lower tension than the parallel boundary, the energies are not hugely different. We would still expect to observe the occasional parallel boundary, but there is no evidence of any in the published TEM images.[16,17] Perhaps the solvent-casting process used to create the experimental samples enhances the preference for the kink boundary. Indeed, solvent should reduce the packing frustration,[36] responsible for the ripples in the thin lamellae. Another potential explanation is that the formation of kink boundaries may have a kinetic advantage. The macrophase separation of the small and large diblocks requires the macroscopic transport of material, and it is understood that the flow of block copolymers happens more easily parallel to the lamellae.[37] Naturally, the boundary would tend to form perpendicular to the flow direction, thus resulting in a further preference for the kink boundary.

There are many directions that future work could take. For instance, it would be useful to investigate how added solvent (or homopolymer) affects the boundaries, as this could very well shed further light on the strong preference for the kink boundary in the experiments of Hashimoto et al.[17] Their experiments also documented other LAM + LAM boundaries, which would be interesting to examine. Furthermore, our calculations could be extended to boundaries between ordered phases of different symmetries, such as lamellar and cylindrical,[38−40] not to mention all the other potential phase combinations exhibited by block copolymer blends.

■ SUMMARY

Self-consistent field theory (SCFT) has been used to examine boundaries (or interfaces) between coexisting lamellar (LAM)

phases in blends of small and large symmetric diblock copolymers. The calculations were performed specifically for the phase diagram in Figure 1, where the segregation strength of the large diblock was fixed at $\chi N_l = 200$ while the relative size of the small diblock was controlled by $\alpha = N_s/N_l$. In particular, we compared the kink boundary (Figure 2b) most commonly observed in experiments[16,17] with the parallel boundary (Figure 2c) suggested by strong-stretching theory (SST). Contrary to SST, the SCFT predicted a lower tension, Γ_b, for the kink boundary consistent with the experimental observations. Furthermore, the predicted morphology nicely agrees with the experimental TEM images in that the ends of the large lamellae induced long-range ripples in the thin lamellae. We also found that, as the critical point is approached, the width of the boundary diverges and the tension vanishes. This may explain why the experiments required a size ratio between the diblocks of at least 1:10 to observe LAM + LAM coexistent, while SCFT predicts that 1:5 is sufficient to cause macrophase separation.

For completeness, we also examined the boundaries at small α, where the short-period LAM phase disorders producing LAM + DIS coexistence. In this case, the tension is lower when the lamellae of the remaining LAM phase are oriented perpendicular to the boundary than when they are parallel. Again this is consistent with what is observed in experiment. Interestingly, the LAM phase induces long-range composition oscillations in the DIS phase, which are well described by a prediction[28] from weak-segregation theory (WST).

This study has provided the first application of SCFT to the boundaries between coexisting phases of a block copolymer blend. The key to the calculation was identifying a finite system box with appropriate boundary conditions (BC's) in which to solve the modified diffusion equations of SCFT. Converging the self-consistent field conditions was also a nontrivial task, particularly because our system had a weak tendency to macrophase separate. Although the grand-canonical ensemble is the natural choice for blends, we had to perform our calculation in the canonical ensemble in order to prevent the boundary from drifting. Depending on the details of the boundary, the calculation may or may not require minimization of the tension with respect to the box size and/or blend composition. The treatment of each boundary has to be considered on an individual basis. Hopefully, our examples will open the door to future studies on the multitude of interesting boundaries exhibited by block copolymer blends.

■ APPENDIX

Here we perform a simple analytical calculation to understand how the kink LAM + LAM boundary behaves as the critical point is approach (i.e., $\alpha \rightarrow \alpha_c^-$). In this regime, the tilt angle, $\theta(x)$, between the lamellar normal and the y-axis varies slowly from $\theta^{(l)} = 0$ to $\theta^{(s)} > 0$ as x increases (see Figure 2). Given that $\theta(x)$ is slowly varying (see Figure 7b), we can then express the tension of the boundary as[8]

$$\Gamma_b \propto \int_{-\infty}^{\infty} \left[\frac{\kappa}{2}\left(\frac{d\theta}{dx}\right)^2 + U(D) \right] dx \tag{13}$$

where the local lamellar period, D, is related to the tilt angle by

$$D = D^{(l)} \cos(\theta) \tag{14}$$

The first contribution in eq 13 comes from the bending energy of the lamellae, for which we assume a constant bending

coefficient, κ, throughout the boundary; this becomes a good approximation near the critical point where the two coexisting phases are very similar. The second term is the compression energy, $U(D) = F - F_{\mathrm{tan}}$, obtained from a calculation like that of Figure 3.

The equilibrium solution for $\theta(x)$ is determined by minimizing eq 13 using calculus of variations. The minimum corresponds to the Euler-Lagrange equation, which can be integrated to give

$$\frac{\kappa}{2}\left(\frac{d\theta}{dx}\right)^2 - U(D) = \mathrm{constant} \tag{15}$$

The resulting constant of integration needs to be set to zero so that $\theta(x)$ converges to a constant in each of the two bulk regions, where $U(D^{(\gamma)}) = 0$ for $\gamma = s$ and l. With that simplification, it follows that the minimization requires

$$\frac{d\theta}{dx} = \sqrt{2U(D)/\kappa} \tag{16}$$

Near the critical point, the compression energy can be expanded as

$$U(D) \approx A + B(\alpha - \alpha_c)(D - D_c)^2 + C(D - D_c)^4 \tag{17}$$

where D_c is the equilibrium lamellar period at the critical point. The critical point occurs when the coefficient of the quadratic term switches sign causing the single minimum at D_c to bifurcate into two minimums at

$$D^{(\gamma)} = D_c \pm \sqrt{\frac{B|\alpha - \alpha_c|}{2C}} \tag{18}$$

where $\gamma = s$ and l correspond to the minus and plus signs, respectively. As usual in these type of Landau calculations, the coefficient of the quadratic term is taken to be linear in the control parameter α, while ignoring any α-dependence in the coefficient of the quartic term. Given that, we require the constant term to be

$$A = \frac{B^2(\alpha - \alpha_c)^2}{4C} \tag{19}$$

so as to satisfy $U(D^{(\gamma)}) = 0$.

The width of the boundary will be proportional to the total change in $\theta(x)$ divided by the maximum rate of change, which occurs at $D = D_c$. Therefore, it follows that

$$w_b \propto \frac{\theta^{(s)} - \theta^{(l)}}{\max\left(\frac{d\theta}{dx}\right)} \propto \frac{\theta^{(s)}}{\sqrt{A}} \tag{20}$$

From eq 14, we have the relation, $D^{(s)} = D^{(l)}\cos(\theta^{(s)})$. Substituting the bulk periods from eq 18 and expanding the cosine function for small angles gives $\theta^{(s)} \propto |\alpha - \alpha_c|^{1/4}$. Inserting this along with eq 19 into our previous expression for the width, it follows that

$$w_b \propto |\alpha - \alpha_c|^{-3/4} \tag{21}$$

To obtain a similar scaling relation for Γ_b, we note that eq 16 allows us to express eq 13 as an integral of $2U(D)$. Thus, the tension, Γ_b, will be proportional to the peak value of $U(D)$ (i.e., A) times the width of the boundary (i.e., w_b), which immediately implies that

$$\Gamma_b \propto |\alpha - \alpha_c|^{5/4} \tag{22}$$

■ AUTHOR INFORMATION

Corresponding Author

*(M.W.M.) E-mail: mwmatsen@uwaterloo.ca.

Notes

The authors declare no competing financial interest.

■ ACKNOWLEDGMENTS

■ REFERENCES

(1) Bates, F. S.; Fredrickson, G. H. *Phys. Today* **1999**, *52*, 32−38.

(2) Abetz, V.; Goldacker, T. *Macromol. Rapid Commun.* **2000**, *21*, 16−34.

(3) Ruzette, A.-V.; Leibler, L. *Nat. Mater.* **2005**, *4*, 19−31.

(4) Matsen, M. W.; Bates, F. S. *Macromolecules* **1995**, *28*, 7298−7300.

(5) Wu, Z.; Li, B.; Jin, Q.; Ding, D.; Shi, A.-C. *Macromolecules* **2011**, *44*, 1680−1964.

(6) Ryu, H. J.; Fortner, D. B.; Rohrer, G. S.; Bockstaller, M. R. *Phys. Rev. Lett.* **2012**, *108*, 107801.

(7) Ryu, H. J.; Fortner, D. B.; Lee, S.; Ferebee, R.; de Graef, M.; Misichronis, K.; Averopoulos, A.; Bockstaller, M. R. *Macromolecules* **2013**, *46*, 204−215.

(8) Matsen, M. W. *J. Chem. Phys.* **1997**, *107*, 8110−8118.

(9) Duque, D.; Schick, M. *J. Chem. Phys.* **2000**, *113*, 5525−5530.

(10) Duque, D.; Schick, M. *J. Chem. Phys.* **2002**, *117*, 10315−10320.

(11) Goveas, J. L.; Milner, S. T. *Macromolecules* **1997**, *30*, 2605−2612.

(12) Wickham, R. A.; Shi, A.-C.; Wang, Z.-G. *J. Chem. Phys.* **2003**, *118*, 10293−10305.

(13) Spencer, R. K. W.; Wickham, R. A. *Soft Matter* **2013**, *9*, 3373−3382.

(14) Zhulina, E. B.; Birshtein, T. M. *Polymer* **1991**, *32*, 1299−1308.

(15) Semenov, A. N. *Sov. Phys. JETP* **1985**, *61*, 733−742.

(16) Hashimoto, T.; Yamasaki, K.; Koizumi, S.; Hasegawa, H. *Macromolecules* **1993**, *26*, 2895−2904.

(17) Hashimoto, T.; Koizumi, S.; Hasegawa, H. *Macromolecules* **1994**, *27*, 1562−1570.

(18) Matsen, M. W. *J. Chem. Phys.* **1995**, *103*, 3268−3271.

(19) Helfand, E. *J. Chem. Phys.* **1975**, *62*, 999−1005.

(20) Papadakis, C. M.; Mortensen, K.; Posselt, D. *Eur. Phys. J. B* **1998**, *4*, 325−332.

(21) According to SST, the enthalpic cost of the LAM + DIS boundary is insensitive to the orientation of the LAM phase, and so the preferred boundaries are the two that do not perturb the chain trajectories in the LAM phase.

(22) Matsen, M. W. *Phys. Rev. Lett.* **1995**, *74*, 4225−4228.

(23) Matsen, M. W. *J. Phys.: Condens. Matter* **2002**, *14*, R21−R47.

(24) Ranjan, A.; Qin, J.; Morse, D. C. *Macromolecules* **2008**, *41*, 942−954.

(25) Matsen, M. W. *Eur. Phys. J. E* **2009**, *30*, 361−369.

(26) Binder, K. *Acta Polym.* **1995**, *46*, 204−225.

(27) Naughton, J. R.; Matsen, M. W. *Macromolecules* **2002**, *35*, 5688−5696.

(28) Fredrickson, G. H. *Macromolecules* **1987**, *20*, 2535−2542.

(29) Leibler, L. *Macromolecules* **1980**, *13*, 1602−1617.

(30) The relationship between exponents occurs because the boundary tension is proportional to the width of the boundary times the height of the energy barrier separating the coexisting phases, which is proportional to $|\alpha - \alpha_c|^2$.

(31) Koneripalli, N.; Levicky, R.; Bates, F. S.; Matsen, M. W.; Satija, S. K.; Ankner, J.; Kaiser, H. *Macromolecules* **1998**, *31*, 3498−3508.

(32) Milner, S. T.; Witten, T. A.; Cates, M. E. *Macromolecules* **1989**, *22*, 853−861.

(33) Birshtein, T. M.; Liatskaya, Y. V.; Zhulina, E. B. *Polymer* **1990**, *31*, 2185−2196.

(34) Matsen, M. W.; Bates, F. S. *J. Chem. Phys.* **1997**, *106*, 2436−2448.

(35) Matsen, M. W. *Eur. Phys. J. E* **2010**, *33*, 297−306.

(36) Matsen, M. W.; Bates, F. S. *Macromolecules* **1996**, *29*, 7641−7644.

(37) Lodge, T. P.; Dalvi, M. C. *Phys. Rev. Lett.* **1995**, *75*, 657−661.

(38) Yamaguchi, D.; Shiratake, S.; Hashimoto, T. *Macromolecules* **2000**, *33*, 8258−8268.

(39) Yamaguchi, D.; Hashimoto, T. *Macromolecules* **2001**, *34*, 6495−6505.

(40) Yamaguchi, D.; Hasegawa, H.; Hashimoto, T. *Macromolecules* **2001**, *34*, 6506−6518.